Haptigami: a fingertip haptic interface with vibrotactile and 3-DoF cutaneous force feedback

Frederic H. Giraud, Sagar Joshi and Jamie Paik

***Abstract*—Wearable fingertip haptic devices aim to deliver somatosensory feedback for applications such as virtual reality, rehabilitation, and enhancing hardware/physical control interfaces. However, providing various kinds of feedback requires several Degrees of Freedom (DoF) and high mechanical complexity which are mechanically difficult to achieve at the mesoscale. Using compliant low-profile transmissions embedded in an origami structure and *PCBmotors* as actuators, we designed and fabricated a novel 3-DoF fingertip haptic device, called *Haptigami*. This underactuated system, measuring 36 x 25 x 26 mm and weighing 13 g, can render vibrotactile and cutaneous force feedback. We tested our device by creating a novel experimental protocol and robotic platform allowing quantitative characterization of mechanical performance. The current prototype of Haptigami produces 678 mN in compression, and 400 mN and 150 mN in shear for the Y and X directions respectively. By virtue of its unique origami-inspired design, Haptigami brings a new direction for future designs of lightweight and compact wearable robots.**

I. Introduction

Somatosensory feedback includes properties such as compliance, texture, pressure, movement and temperature, fundamental for perceiving our surroundings. The field of Haptics aims at better understanding this type of feedback, in order to artificially recreate these sensations to the user. This has led to numerous advances in Human Machine Interactions (HMI) [1], rehabilitation [2], [3], robotic control [4], and exploration of virtual world [5]. In particular, there has been a flourishing interest in haptic devices for the fingertips, due to their high sensitivity and importance in manipulation. Existing fingertip haptic devices have a wide range of designs depending on the number of degrees of freedom (DoF), type of haptic feedback, and wearability. While bench-top grounded devices can typically offer more modalities, there are additional benefits to wearable devices as they allow to extend their functionalities to "out-of-the-lab" environments and therefore everyday life.

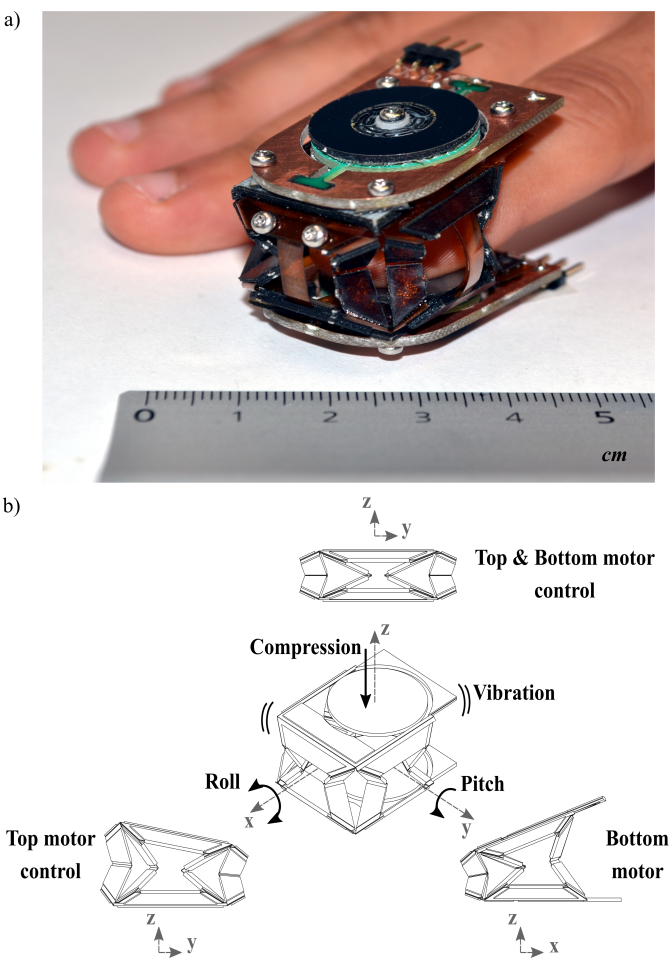

Fig. 1. Haptigami presentation: a) pictured on the user's fingertip; overall dimensions: 36 x 25 x 26 mm and 13 g. b) Haptigami renders vibrotactile and 3-DoF cutaneous feedback

Pacchierotti et al. [6] conducted a concise review of current wearable haptic devices. While a large number of devices only produce vibrotactile feedback [6]–[8], many systems provide 3-DoF cutaneous feedback, including compression, roll and pitch motions, via a parallel mechanism that manipulates a small platform in contact with the fingertip [9]–[14]. One such device has additional mechanisms that provide haptic feedback to the entire finger [15]. Young et al. [16] presented a 6-DoF device (three positions and orientations), while Gabardi et al. [17] developed a 3-DoF device with a voice-coil that can provide vibrotactile feedback. However, as most of these devices are made using conventional mechanisms consisting of DC motors, linkages and joints, the additional capabilities are at the cost of increased weight, size and design complexity. This trade-off in the design of such devices has been summarized well in a recent review paper by Culbertson et al. [18]: "Can we enable consumer haptic devices by decreasing cost, size and weight, and power requirements, potentially via the use of novel actuators and smart materials?". One such example is the SPA-skin by Sonar et al. [8], which embeds actuation and sensing into soft, hyper-elastic materials providing force tunable vibrotactile feedback up to 100 Hz with a device of only 1 mm thick. However, the use of stretchable materials hinders the number of DoF, preventing applications with more diverse types of haptic feedback. While designing compact devices capable of producing multiple actuation modes is one challenge, understanding their mechanical behaviour is also necessary. However, most papers assess the performance of their devices using user studies only, that shows the effectiveness in delivering the desired feedback [18]. Only a few

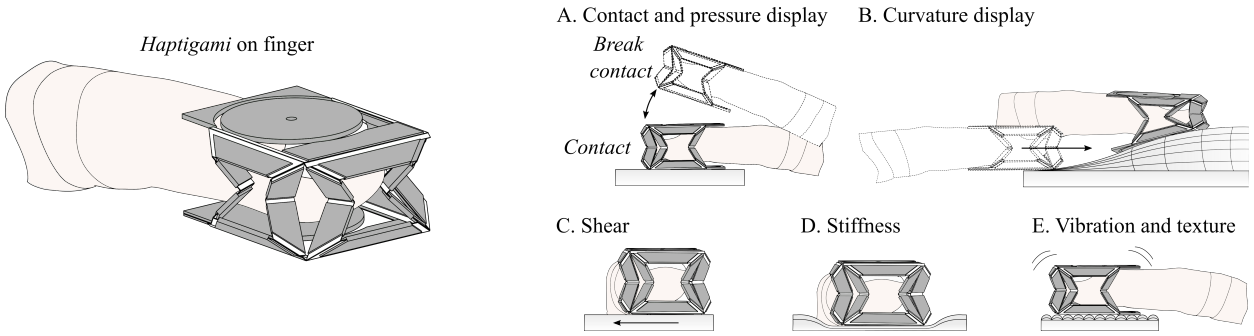

Fig. 2. Located at the fingertip, Haptigami is mechanically capable of rendering five types of cutaneous stimuli: A. display contact and pressure, B. curvature, C. shear force, D. stiffness, and E. vibrotactile feedback.

research studies characterize the mechanical force output of their device, albeit in a very limited range of motion [15], [19]. Therefore, although actuation levels are controllable, it is difficult to estimate how much force the user actually feels. Thus, in addition to design innovations for reducing bulk, there is a need to create a link between the multidimensional force output and perceived sensation by the user, in order to establish models and improve design and development of future haptic devices.

Recently, researchers in robotics have started exploring a new origami-inspired design approach, which combines flexure mechanisms with unconventional actuators using 2D layer-by-layer manufacturing techniques to create compact, scalable and highly customizable robots, a.k.a Robogami [20]–[26]. These properties make Robogamis a viable option for developing fingertip haptic devices. However, in its current form, Robogami cannot be directly implemented for wearable Haptics. For instance, actuation methods in Robogami mostly include shape memory alloys [24] or pneumatic pouch motors, which suffer from limitations in terms of precise control, reversible motion and bandwidth. Mintchev et al. [27], have addressed these using DC motors to create a haptic joystick, but at the cost of increased bulk and reduced wearability. In addition to the motors themselves, this increased bulk is also due to the mechanisms required for transmitting force and displacements. We have addressed this challenge in our previous work [28] by designing low-profile slider-crank and cam-follower transmissions, powered using flat piezo-motors [29], [30]. These mechanisms, measuring only 4.75 mm thick with the motor and transmissions, are compliant such that they can transfer forces out of plane.

In this paper, for the first time, we integrate this concept into a novel, compact fingertip haptic device called *Haptigami* (Fig. 1a), capable of delivering vibrotactile and 3-DoF cutaneous feedback. Our system benefits from two low-profile, high-force density piezomotors connected to low-profile slider-crank mechanisms, all integrated in an Origami-inspired base structure. Haptigami consists of four such mechanisms, arranged, stacked, motorized, and finally assembled into the final 3D structure. The resulting device is the smallest (36 x 25 x 26 mm) and most lightweight (13 g) fingertip haptic device, as compared to devices providing similar types of feedback. To quantitatively assess the mechanical performance of Haptigami, we developed a novel experimental protocol and a 5-DoF robotic platform to characterize the force output in its full range of motion. Contrary to the commonly used user-surveys, this method allows to objectively measure mechanical performance of meso-scale systems and can be readily implemented with most other fingertip haptic devices. This paper is a step towards a new paradigm in the design and fabrication of compact haptic devices capable of providing multiple modes of somatosensory feedback to the user.

The main contributions of this work are:

- *Haptigami*, the first instance of using origami robotics in wearable haptics, which makes it the smallest and lightest fingertip haptic device capable of roll, pitch, compression and vibration.
- Comprehensive modeling and closed-loop control of the kinematics of *Haptigami* that relates motor rotations (inputs) to roll, pitch and compression (controllable outputs) of the device.
- A new experimental protocol for characterizing the force vs. displacement behaviour of the meso-scale haptic devices in their entire range of motion and all actuation modes (roll, pitch, compression, shear, vibration).

II. Haptic feedback of wearable fingertip devices

A device capable of rendering several types of interaction enhances the immersive experience in a virtual world, offering multiple modalities such as size, shape, rigidity and texture, to perceive its surroundings. Our objective was to develop a compact and lightweight device that can achieve five different types of haptic feedback: *A. contact and pressure display, B. curvature display, C. shear forces, D. stiffness, and E. vibration and texture* (Fig. 2). From a kinematic point of view, each type of feedback can be achieved with a single or a combination of six mechanical capabilities of the device, which include linear motion in the X and Y direction, compression, pitch, roll and vibration; explained as follows:

A. **Contact display** This kind of feedback allows making and breaking of contact with the user, with control on the contact location. The former requires compression, whereas the latter additionally needs lateral displacement for simulating contact location, hence requiring between one and three mechanical

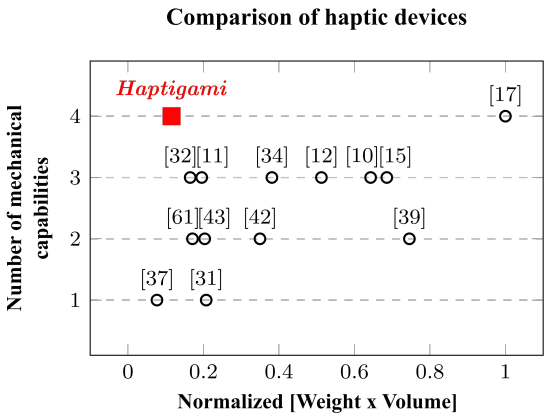

References:

[10] [15] *Chinello et al.* 3-RRS cutaneous device

[11] *Leonardis et al.* 3-DoF asymmetric 3-RSR kinematics device

[12] *Schorr and Okamura* 3-D skin deformation as force substitution

[17] *Gabardi et al.* Render of virtual shapes and surface features

[31] *Scheggi et al.* Leap motion and tactile device

[32] *Tsetserukou et al.* 5-bar linkage mechanism for 2-DoF force feedback

[34] *Prattichizzo et al.* 3-DoF device for cutaneous force feedback

[37] *Frediani et al.* Display for virtual interactions with soft bodies

[39] *Minamizawa et al.* Gravity grabber for virtual mass sensation

[42] *Gleeson et al.* Tangential skin displacement display

[43] *Girard et al.* Haptip: haptic shear forces display

[61] *Solazzi et al.* 2-DoF device for tangential skin displacement

Fig. 3. Comparison of Haptigami with state-of-the-art haptic devices in terms of number of mechanical capabilities and wearability. The latter is defined here as normalized Weight x Volume.

capabilities. To achieve this, some existing devices have used moving platforms in contact with the fingertip [10]–[12], [15]–[17], [31]–[34], pin arrays [35], [36], soft inflatable systems [37], [38] or a belt underneath the finger [39], [40]. Among these, [10]–[12], [15]–[17], [32], [33], [35], [36] can control the location of the contact-point by means of additional DoFs, but at the cost of increased bulkiness.

B. **Curvature display** This display aims for users to feel the curvature change of a surface, allowing exploration and shape perception of objects. To attain this effect, existing devices orient the pitch and roll of the platform in contact with the fingertip [10], [15]–[17], [33], [34], [41]. Similarly, [35], [36] used the compression from a pin array individually controlled in height to create a curved surface. Therefore, this feedback requires at least two mechanical capabilities.

C. **Shear forces** This type of feedback conveys information about the shear forces acting on the fingertip while it interacts with its surroundings [18]. Shear forces can also simulate the weight of an object grasped by the user [39]. This cutaneous stimulus requires a structure able to render lateral displacement and hence between one and two mechanical capabilities. Some parallel mechanisms use a tactor, which moves in a plane [33], [42], [43], or pulls a flexible material [39], [40] underneath the finger to produce this effect.

D. **Stiffness** Stiffness sensation comes from the material mechanical reaction to a deformation induced by the user by application of force. Traditionally, such haptic feedback uses externally grounded devices that apply a net external force on the finger [44]. However, authors of [12] showed using a user survey that a normal skin deformation device worn on the fingertips can also render this sensation. By extending this principle, several devices with normal displacement or force modulation of the element in contact with the fingertip [10]–[12], [15]–[17], [32], [34] and soft inflatable actuators [37] are capable of this type of feedback using one to three mechanical capabilities.

E. **Vibration and Texture** Vibrotactile feedback is among the most widely studied haptic feedback. By controlling the vibration based on the movement, it is possible to produce sensations of texture [45]. Vibrotactile feedback often provides notification with small and lightweight actuators [46]–[48]. Some studies [17], [36], couple vibrotactile to contact and curvature displays to form perceptual cues, simulating different materials and textures. Hence this requires one to three mechanical capabilities depending if the vibration is coupled with a lateral displacement.

The effectiveness of wearable haptic interfaces is affected by several factors [6] that include speed, force, workspace, size, weight and impairment. A high number of mechanical capabilities and degrees of freedom is often directly proportional to the overall size and weight of a device due to the added motors and transmissions. A larger device reduces user's dexterity and limits multi-finger tasks. A heavier device leads to fatigue, and interferes with the haptic force feedback. To visualize this, we made a comparison table of the current state of the art haptic devices in Fig. 3. The X-axis represents the device's bulkiness, using a metric defined as the normalized product of weight and volume. The Y-axis is the number of mechanical capabilities a device can achieve (pins arrays rely on a different principle to generate haptic feedback, we did not include them in this graph). We see from the figure that there is a clear trend towards increasing bulk with the number of mechanical capabilities. This suggests that in existing devices, more mechanical capabilities often result in a bulkier and therefore less wearable device.

Here, we present *Haptigami*, a scalable and lightweight haptic platform that benefits from multi-material 2D fabrication methods for compliant, low-profile actuation. It consists of an origami-inspired parallel mechanism structure powered by piezo-motors and embedded slider-crank transmissions, which can produce vibrations and move in 5 DoF by virtue of its under-actuated design. However, as the current design is unable to uncouple shear from pitch and roll displacement, it can effectively provide four mechanical capabilities: pitch, roll, compression and vibration. By providing contact and stiffness display via compression, shear and curvature display via roll

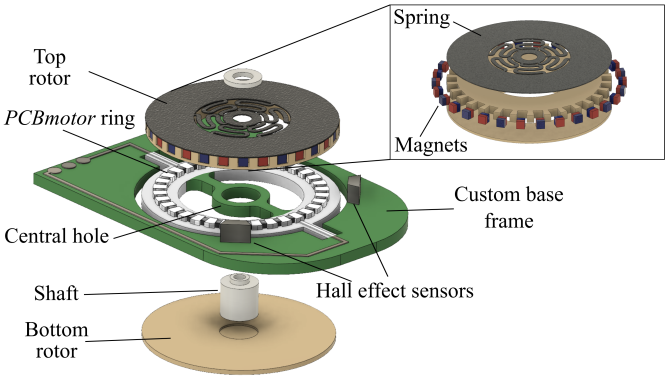

Fig. 4. Fully integrated actuator with *PCBmotors* implemented on a custom PCB. Hall-effect sensors read the top rotor's magnets alternated polarity to control rotation angle and direction. A spacer glued onto the bottom rotor allows maintaining the two rotors in the center and synchronizing their rotation. As this is a friction-based actuator, a flat spring enables keeping a constant contact force between the rotors and stators.

and pitch, and texture via vibration, the Haptigami is mechanically capable to produce all cutaneous stimuli described in Fig. 2. At the same time, its novel and low-profile design makes it relatively compact as compared to existing devices. Fig. 3 shows Haptigami appearing as an outlier, combining high number of mechanical capabilities with among the smallest normalized weight x volume.

III. Design and Fabrication of an Origami-Inspired Haptic Platform with Integrated Transmissions

The unique design of Haptigami allows to achieve a higher number of functionalities without compromising size and weight. This section describes Haptigami working principle and design of its three major components: piezomotors, embedded slider-crank transmission and an origami-inspired base structure.

A. Actuation and closed-loop control of the piezomotors

For actuation, we use piezomotors stator manufactured by *PCBmotor* [29] with a custom frame, a rotor and a sensing system. The piezomotor consists of a stator in the form of a PCB and is composed of piezo-crystals arranged in a circle on its two faces. We attached two rotors with flat circular faces, above and below the stator, held together by a spring-loaded shaft. The piezomotor generates a traveling wave along the crystals, which drives the rotor via friction. It is low-profile with a high-force density, making it suitable for actuating Robogamis. We use a piezomotor of 20 mm diameter for Haptigami. As per the PCBmotors datasheet, it provides a free speed of 96 rev/s, 8 Nmm stall torque and a maximum output power of 40 mW.

We cut out the stator's circular ring from the 20 mm PCBmotor, containing the piezo crystals, represented in white in Fig. 4, and placed it on a custom-made base frame via bridges. The base frame also has a central hole to support the shaft connecting the top and bottom rotors. We fixed the bottom rotor rigidly to the shaft, and a customized low-profile spring fabricated from a 0.1 mm steel sheet by laser machining,

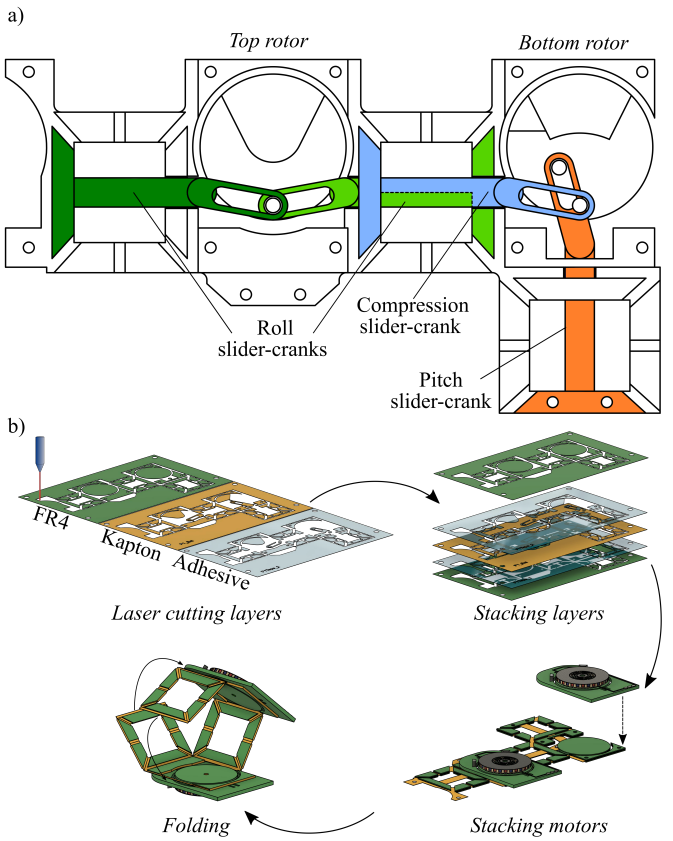

Fig. 5. Haptigami's mechanism and fabrication: a) Internal structure composed of four low-profile slider-crank mechanisms connected to the three waterbomb patterned sides (two slider-cranks control the same side, allowing compression). Each motor can actuate two independent transmissions and select the one to drive with its sense of rotation. b) Manufacturing process: after laser cutting the Kapton, FR4 fibre-glass and Polymelt layers, we aligned them and fixed them together by heat pressing. Then we mounted the actuators on top of the rotors already created as the layer stack. Finally, the folding joints allow folding this 2D structure into the 3D device.

connected the top rotor. The spring tension maintains an optimal contact force between the stator and rotors, critical for this friction-driven system. We use two of these customized piezomotors as the actuators for Haptigami.

We personalized a quadrature encoder to enable closed-loop control of the piezomotor described above. It consists of two bipolar Hall-effect sensors positioned on the stator, and thirty 1x1x1 mm^3 square magnets placed with alternating polarity on the side of the rotor. During rotation, the Hall-effect sensors generate two quadrature PWM outputs that go to the microcontroller (Arduino Mega) through a custom designed electronic low-pass filter. The Arduino's interrupts extract rotation angle and direction, with a resolution of 6°, and uses them as the bang bang controller input to drive the motors. According to the model presented in section IV, this resolution translated to values ranging from 3.4° to 4.4° in roll, 0.12° to 2.1° in pitch and 0.83 mm in compression. The motor driver, supplied by PCBmotor, generates the signal that drives the piezo crystals of the stator. Fig. 4 illustrates this flat actuator system.

B. Low-profile compliant slider-crank mechanism

In order to generate useful movement from a piezomotor, we developed a novel low-profile and compliant slider-crank transmission described in [28]. The connecting rod, composed of two Kapton layers of the same thickness and glued using Polymelt adhesive, drives the slider that consists of a single 50 μm Kapton layer. We attached the other end of the connecting rod to the bottom rotor of the piezomotor, which acts as the crank. During the pulling phase, our transmission functions similarly to that of a traditional slider-crank. However, during the pushing phase, the flexible elements cannot transmit the motion due to buckling, which may damage the mechanism. To avoid this problem, we introduced a slot in the rod, which allows decoupling the two phases. We use four such slider-crank mechanisms to generate pitch, roll and compression, as shown in Fig. 5a.

C. Origami-inspired base structure with embedded transmissions

The base-structure forms the main body of Haptigami and embeds the transmissions described above. The origami design developed in [27] inspired the base structure. It consists of 27 distinct layers: (i) three 0.2 mm FR4 fiber-glass layers, (ii) one 0.3 mm FR4 layer, (iii) ten 0.05 mm Kapton and (iv) thirteen Polymelt 701 layers. The first thirteen layers include the blue and dark green slider-crank mechanisms, while the remaining thirteen contain the light green and orange slider-crank presented in Fig. 5a. We adopted a four-step manufacturing process (Fig. 5b) as described in [28]. After laser cutting the different layers, we stacked them using pins and then glued them together using a heat press to create the 2-D assembly of the device. Finally, we added the actuators of Section III-A and folded the 2-D assembly using the flexure joints into the 3-D Haptigami, measuring 36 x 25 x 26 mm and weighing only 13 g.

The final structure consists of a top and bottom face connected on three of its edges using a type of origami structure called waterbomb [49], which acts as a spring and helps the device to retain its shape when the piezo motor is not active. The fourth side of the mechanism is open, allowing insertion of the finger. The top and bottom faces of the structure hold the piezomotor, while the sliders of the four slider-crank mechanisms act as tendons to generate the motion. The compliance of the adopted materials enables the slider-crank mechanisms to transmit motions and forces out-of-plane.

D. Working principle

The presented low-profile Haptigami design is capable of generating roll, pitch, and compression motions and vibrotactile feedback. We use the two piezomotors and four slider-crank mechanisms described above to drive them. Each motor controls two slider-crank mechanisms, thanks to the decoupling between pushing and pulling phases. We select which of the two transmissions to drive by choosing the motor's direction of rotation. As roll and pitch are connected to different motors, they can be achieved simultaneously. The roll, pitch and compression motions achieved by Haptigami, along with the corresponding motor commands, are described in Table I:

TABLE I
HAPTIGAMI MOTION ACHIEVED THROUGH MOTORS DIRECTION OF ROTATION, CLOCKWISE (CW) OR COUNTERCLOCKWISE (CCW)

Top motor direction	Bottom motor direction	Haptigami motion
ccw	-	roll(+)
cw	-	roll (-)
-	cw	pitch (+)
ccw	ccw	compression

As the table describes, it is not possible to achieve compression and pitch simultaneously, since compression required the use of two motors. In order to generate vibrotactile feedback, we alternate the direction of the piezomotors at high frequency. The direct contact with the user and low inertia aid in transmitting the vibrations to the user's finger with little loss. Thus, the proposed novel robotic platform is capable of producing vibrotactile and 3-DoF force haptic feedback.

IV. KINEMATIC MODEL OF HAPTIGAMI

To achieve the various types of haptic feedback described in Section II, it is necessary to understand the motion and force capabilities of Haptigami. However, as it consists of non-conventional joints, links and actuators, conventional models cannot be directly implemented for position control. Similarly, the inherently compact and compliant structure also makes it difficult to assess the force applied by the device on the user. Therefore, in this section, we derive a kinematic model adapted to our structure and apply it to achieve closed-loop control. In addition, we develop a novel experimental protocol and setup to quantitatively characterize Haptigami for its blocked force in all kinematic configurations of the workspace, and its vibrotactile feedback. We used the high-level dynamic programming language, *Julia* [50] to analyze all the experimental data.

Haptigami consists of an origami structure, actuated by piezomotors driving the embedded slider-crank mechanisms. As the piezomotors rotate, the slider, acting as the tendon, pulls on the base structure to create movement. In this section, we develop and validate a kinematic model for this mechanism, and apply it for closed-loop control of Haptigami.

A. Kinematic model

Kinematics of most fingertip haptic devices do not change when worn on the finger as they consist of rigid segments and joints [34], [51]. Wearing Haptigami or not changes its kinematics due to its compliant nature. For a realistic kinematic analysis, we could use true geometry of the finger as the constraint for deriving the kinematics. In this paper, we model the contact surface to a sphere approximating the fingertip to derive the kinematics equations. This assumption is valid for our analysis because the phalanx does not affect the kinematics since Haptigami pitches only in the forward direction.

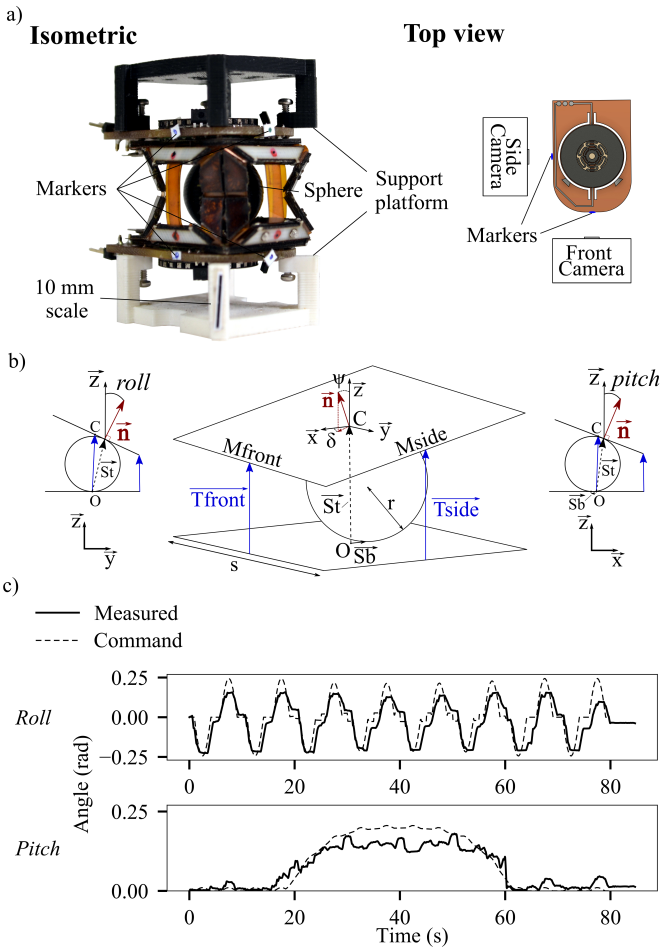

Fig. 6. Haptigami's kinematic model and closed-loop control experiment and results: a) Experimental setup used to verify kinematic model; We fixed Haptigami on a support platform with a 3D-printed sphere inside and used a front and side cameras to record the marker positions, deducing the tendon lengths and platform orientation. b) We model our system as two plates with a sphere inside, representing the user's finger contact point and determine the motion of the two plates by the sphere and tendon lengths. c) Comparison between model and the measured values of roll and pitch angles.

We model Haptigami as two squares with equal dimensions and of side length s, as presented in Fig. 6b. The bottom face is grounded, while the top face is free, with O and C representing the coordinates of their square centers. The sphere, placed between the two faces, is fixed to the bottom face, with vector $\overrightarrow{S_b} = (-Fpos, 0, 0)$ representing the point of contact. $Fpos$ is the distance between the square's center and sphere contact point on the bottom square. We assume the top face to freely slide and roll over the sphere, with the point of contact given by vector $\overrightarrow{S_t} = \overrightarrow{S_b} + r \cdot \overrightarrow{z} + r \cdot \overrightarrow{n} = (x_0, y_0, z_0)$:

$$x_0 = r \cdot n_x - Fpos; \quad y_0 = r \cdot n_y; \quad z_0 = r \cdot n_z + r \tag{1}$$

where n_x, n_y and n_z are x, y and z components, respectively, of the unit vector $\overrightarrow{n}$, normal to the upper platform. Using spherical coordinates, $\overrightarrow{n}$ is defined as $\overrightarrow{n} = (\sin(\psi) \cdot \cos(\delta), \sin(\psi) \cdot \sin(\delta), \cos(\psi))$.
Using the above equations, the plane corresponding to the top face is given by

$$n_x \cdot (x - x_0) + n_y \cdot (y - y_0) + n_z \cdot (z - z_0) = 0 \tag{2}$$

We define Haptigami's motion as the relative motion between the top and bottom faces denoted by the Cardan angles roll and pitch, calculated as follows:

$$roll = \frac{\arccos(\psi)}{\sqrt{\sin^2(\psi) \cdot \cos^2(\delta) + \cos^2(\psi)}} \tag{3}$$

$$pitch = \frac{\arccos(\psi)}{\sqrt{\sin^2(\delta) \cdot \sin^2(\psi) + \cos^2(\psi)}} \tag{4}$$

Controlling the tendon lengths, powered by the piezomotors allows achieving this motion. The vectors $\overrightarrow{Tfront}$ and $\overrightarrow{Tside}$, which are connected at the mid-points, *Mfront* and *Mside*, of the top face edges represent these tendons.

$$\overrightarrow{Tfront} = \begin{bmatrix} 0 \\ (s/2) \cdot (1 - \cos(roll)) \\ Tside_z + (s/2) \cdot \sin(roll) \end{bmatrix} \tag{5}$$

$$\overrightarrow{Tside} = \begin{bmatrix} (s/2) \cdot (1 - \cos(pitch)) \\ 0 \\ Tfront_z + (s/2) \cdot \sin(pitch) \end{bmatrix} \tag{6}$$

As points *Mfront* and *Mside* lie on the top face, they satisfy (2).

$$\begin{aligned} n_x \cdot Mside_x + n_y \cdot Mside_y + n_z \cdot Mside_z = d \\ n_x \cdot Mfront_x + n_y \cdot Mfront_y + n_z \cdot Mfront_z = d \end{aligned} \tag{7}$$

where $d = n_x x_0 + n_y y_0 + n_z z_0$. The set of equations (1) to (7) gives the kinematics of Haptigami that relate the inputs, $\|\overrightarrow{Tside}\|, \|\overrightarrow{Tfront}\|$, to the outputs, *pitch*, *roll* or ψ and δ. The forward kinematics are difficult to derive due to the complexity of the equations required to isolate ψ and δ. To address this, we use the numeric solver NLsolve.jl [52] which gives the correct angle in an average time of 1ms after the first compilation. Solving (7) gives the reverse kinematics:

$$\begin{aligned} \|\overrightarrow{Tfront}\| = &(((\cos(pitch)s - s - 2Fpos)\cos(\delta) \\ &- s\sin(\delta))\sin(\varphi) \\ &+ (-\sin(pitch)s + \\ &2r)\cos(\varphi) + 2r)/(2\cos(\varphi)) \end{aligned} \tag{8}$$

$$\begin{aligned} \|\overrightarrow{Tside}\| = &(((-s - 2Fpos)\cos(\delta) + s\sin(\delta) \\ &(\cos(roll) - 1))\sin(\varphi) \\ &+ (-\sin(roll)s + 2r)\cos(\varphi) \\ &+ 2r)/(2\cos(\varphi)) \end{aligned} \tag{9}$$

Additionally, we determine the top plate's centre coordinates as follows:

$$\begin{aligned} \overrightarrow{OC} = &\frac{\overrightarrow{OMside} + \overrightarrow{OMfront}}{2} \\ &+ \frac{\overrightarrow{OMside} - \overrightarrow{OMfront}}{2} \times \overrightarrow{n} \end{aligned} \tag{10}$$

Finally, to control the interface, we converted the tendon lengths into rotation angles of the driving piezomotors using the conventional offset slider-crank kinematic equations that

relate the motor rotation angle θ, to the tendon length t, as explained in [28]. The slider position x of a slider-crank mechanism, which is a measure of the tendon length, is given by:

$$x = a \cdot \cos(\theta) + b \cdot \cos(\mu(\theta)) \tag{11}$$

with

$$\mu(\theta) = \arcsin(\frac{a \cdot \sin(\theta) - c}{b}) \tag{12}$$

where a, b and c, are the crank, rod and offset size, respectively and μ is the angle between the connecting rod and the slider. We solve the above by using a solver in [53] to get the equation for $\theta(x)$, and we use this equation directly in the control.

B. Kinematics validation

Here, we control the piezomotors of Haptigami and compare the achieved pitch and roll motions to those predicted by our kinematics model. We placed a sphere (diameter = 14 mm) inside our prototype at $\overrightarrow{S_b} = (-Fpos, 0, 0) = (-2, 0, 0)$, to represent a finger as seen in Fig. 6b. Using optical markers and two cameras as shown in Fig. 6a, we measured the spatial position of Haptigami's top face with respect to the bottom face. To reduce the visual distortion effect on the results, the cameras were put at a distance where the motion of the markers is centered and focused. At this distance, the resolution was 0.05 mm by pixel.

The top motor is responsible for generating the pitch motion, while the bottom motor is responsible for the roll. We simultaneously sent two sines waves as control signals, traversing the entire rotation range of Haptigami and corresponding to oscillating in both roll and pitch directions. We tracked these reference signals by closed-loop control of the piezomotors using feedback from our custom encoders presented in Section III-A. We used the auto-tracker *CSRT* algorithm of *OpenCV* [54] for analyzing the video to get the optical marker positions. The performance of this tracking method is assessed in [55] and is more than sufficient for our application due to our low speeds and displacements. The data was acquired at a framerate of 25 fps, then low-pass filtered at 3 Hz.

Fig. 6c compares the measured pitch and roll angles of Haptigami to those predicted by our kinematics model. We see that the measured values match our model during the pitch activation time interval from 18 to 60 s, with a root mean squared error of 0.055 rad. We observed a slight reduction in the measured maximum amplitude, which can be attributed to the compliance of the waterbomb structures, affecting the transmission efficiency. In addition, we also observe a higher cross-influence of pitch and roll angles as compared to the model. Overall however, for the approximation of the fingertip as a sphere, our model accurately achieves closed-loop control of the pitch and roll, using the embedded hall sensors.

Additional geometrical and mechanical parameters such as more complex finger shape, skin deformation under pressure, and contact point compliance need to be considered for an updated version of the model. Using a plastic sphere as an approximation of the fingertip allows working with straightforwards kinematic equations. Abdouni et al. [56], found the Young's modulus of the fingertip's skin to vary between 20 and 100 kPa in shear, leading to negligible displacements (around 0.02 mm) with the Haptigami shear forces values given by Table II. The same Table gives us the maximal normal force of 693 mN that corresponds to a normal finger deformation of around 1.2 mm according to Dzidek et al. [57]. We estimate the error induced by this deformation by reducing the sphere radius of our current model. This leads to an RMS value of 0.077 rad, which is significant and should be included in a future model. Finally, frictions that differ between plastic sphere and skin could also create disturbances.

C. Maximal roll and pitch frequencies

To measure the Haptigami's maximum roll and pitch frequencies, we programmed the roll and pitch motors to rotate between their upper and lower limits as fast as possible. We recorded a video of the resulting Haptigami motion and extracted the times when the Haptigami reaches its extremes positions. The roll motion between $\pm$ 0.24 rad and the pitch motion between 0 and 0.20 rad have a frequency of 1.6 and 1 Hz respectively. The pitch speed is slower than the roll due to its slider-crank design as shown by Fig. 5 that requires a larger rotor rotation for the same slider displacement.

V. Force characterization

Mechanical characterization of any fingertip haptic device is challenging due to the arbitrary physical grounding of the device and preloaded conditions. Here, we present a novel experimental protocol and platform for a quantitative evaluation of meso-scale devices, which can be customized in range and resolution for the target application.

A. Experimental setup

Similar to the protocol escribed in [58], we attach the Haptigami onto a bench-top setup, enforce displacement in its range of motion, and measure the blocked forces while powering the two piezo-motors. We accomplish this using a 5-DoF robotic platform as shown in Fig. 7a. It consists of three linear motors or stages, capable of enforcing linear displacement in X, Y and Z axis and a pan-tilt mechanism consisting of two servomotors for roll and pitch motions. We affixed the bottom face of Haptigami to the X-Y stages, and the top plate to the pan-tilt mechanism which in turn is fixed on the Z stage as seen in Fig. 7a. By controlling these linear motors and pan-tilt mechanism of the characterization platform, we enforce the desired displacement in XYZ and roll-pitch respectively, to the top plate of the Haptigami. This displacement is based on the model described earlier in Section IV-A, assuming a spherical shape for the finger. To calculate the control inputs for the various stages of the characterization platform, we must calculate the individual displacements required in five directions. For the roll and pitch, these values are exactly the same as the roll and pitch angles of the Haptigami. To calculate control values for the X, Y and Z stages, we consider the X-Y displacements of the Haptigami top plate, as well as those of the pan-tilt mechanism, occurring due to its non-zero arm lengths.

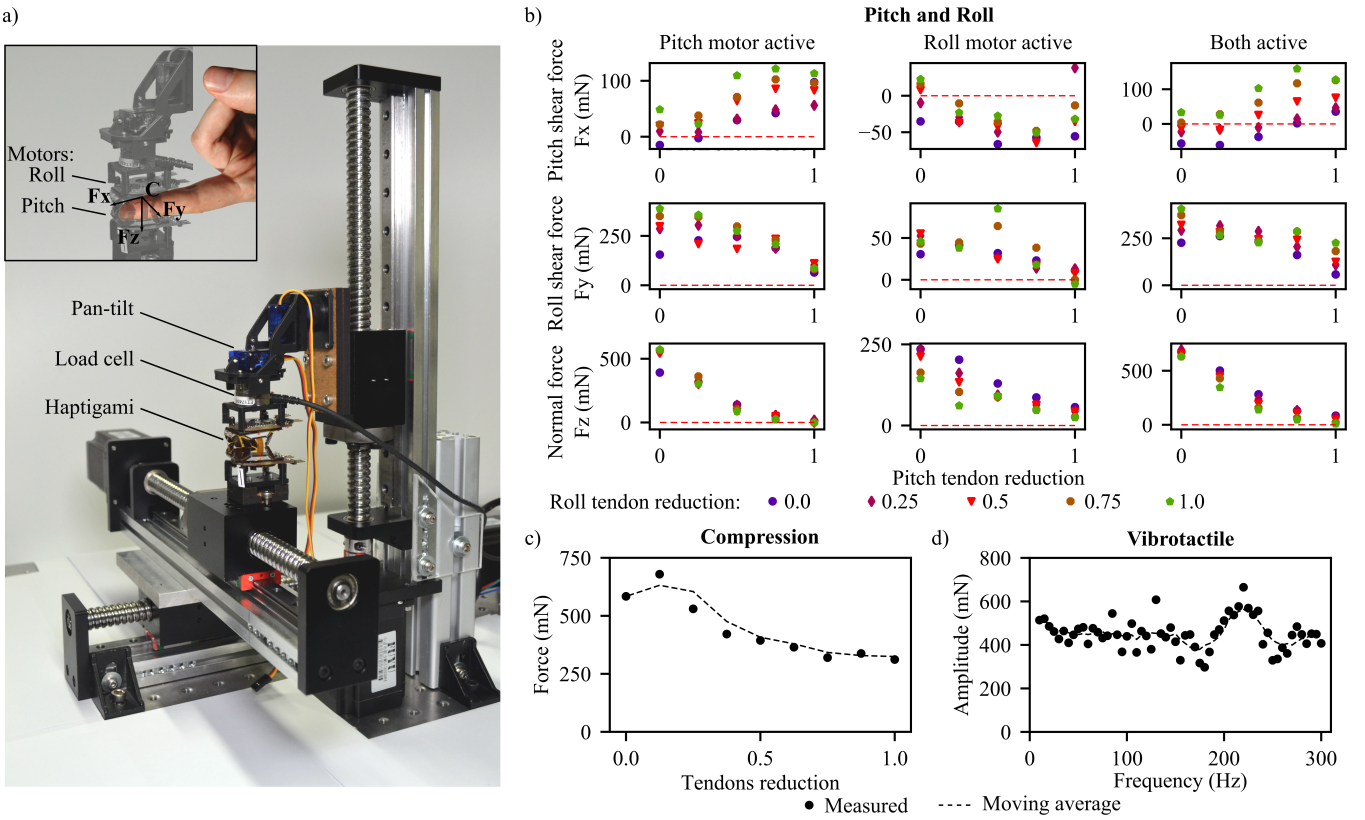

Fig. 7. Force characterization setup and results: a) Force characterization setup simulating the platform on a finger; we fixed the Haptigami to the 5-DoF platform in direct contact with the 6-DoF load cell. b) For every orientation of its workspace, we measured the force along XYZ axis depending on the actuated motors. The configuration is defined from the normalized tendon length reduction that corresponds to how much the tendon has been pulled by the slider-crank. c) Compression experiment, we attached Haptigami to the platform with a null angle. For different heights, we actuated the roll motors and measured the compression force. d) Vibration experiment, we attached Haptigami to the platform with a null angle and control the top motor to move back and forth at different frequencies and measure the amplitude of the resulting signal.

While enforcing the displacement, we measure the blocked force of Haptigami using a *Nano17* 6-axis force sensor from *ATI Industrial Automation* (force resolution = 12.5 mN), attached between the top face of the Haptigami and the pan-tilt mechanism as seen in Fig. 7a. We used a custom Labview program to measure the load-cell data, and to send instructions to the Arduino Mega, which then controls the 5-DoF platform. Lastly, during characterization, we activate the two motors of the Haptigami, also using the Arduino Mega. With this setup, we moved Haptigami to different configurations in its range of motion and characterized it in three scenarios: (i) compression motion (ii) roll and pitch motions (iii) vibrotactile feedback.

B. Pitch and roll

As seen in Section IV-A, the Haptigami motion is a result of shortening of the tendon lengths. We therefore represent its displacement using its input space defined via its tendon length reduction:

$$normalized\,tendon\,reduction = \frac{L_0 - L}{L_0}$$

where L is the current tendon length and L_0 is maximal tendon length, in mm. We displaced the Haptigami in a set of points defined by a grid of 5 x 5, where each grid point corresponds to the front and side tendon lengths, with a maximum value of 2 mm on each side. This motion corresponds to a total pitch of $+10°$ and roll of $+12°$, assuming a sphere of 14 mm diameter placed inside. We calculated the spatial orientation (x, y, z, δ, ψ) of Haptigami at the grid points using the kinematic model described in Section IV-A and converted into a set of instructions for the 5-DoF robotic platform. For every grid point, we used the following protocol: 1. Move Haptigami to a new position, 2. Activate pitch motor, 3. Activate roll motor, 4. Activate both motors. We programmed each motor activation to last two seconds and then come back to the initial position.

Fig. 7b shows the measured forces vs. normalized tendon length reduction of Haptigami. The Y axis represents the measured forces, while the X axis and different markers represent displacements in the pitch and roll directions respectively, expressed in normalized tendon lengths. These forces are generated by the front and side tendons pulled by the pitch and roll piezo-motors respectively. Therefore they depend on the relative orientation of the tendon force with respect to the top face, as well as its magnitude, which depends on the torque of the piezo-motor and orientation and design of the slider-crank mechanism.

With increasing displacement in the pitch direction, the component of the tendon force $\overrightarrow{Tfront}$ in the X axis increases.

This leads to an increasing pattern of force vs. displacement for X direction and a decreasing one for the Y and Z directions, as seen in the first column of Fig. 7b. A similar pattern is expected for the roll direction, but the measured data does not completely follow this, as seen in the second column of Fig. 7b. This deviation could be attributed to mechanical interference in the compliant transmissions due to the fact that both motors contribute to the roll motion. The third column of Fig. 7b corresponds to both motors active, pulling in roll and pitch directions. Therefore, the plots are somewhat equal to the sum of the first two columns, which we found was especially true for Fz. Another observation is that the forces are generally higher for pitch motor active, as compared roll motor active. This is because the crank radius for the slider-crank mechanism is smaller for the former as compared to the latter, as described in Section III. Lastly, due to the underactuated and coupled design of the Haptigami, we see from the third row of Fig. 7b that shear forces are always accompanied by compression forces. The maximum forces are 690 mN in normal force, 407 mN in shear roll and 159 mN in shear pitch.

C. Compression

We controlled the characterization platform to only move its Z stage, and displaced Haptigami from an initial height of 20 mm to a final height of 16 mm in steps of 0.5 mm. We activated both motors according to Table I and measured the maximum compression force at each step, held for 2 s. Fig. 7c shows the measured force, with the X-axis denoting the displacement expressed as normalized tendon length. We see that the compression force slightly reduces with increasing displacement, with a maximum value of 678 mN.

D. Vibrotactile feedback

As explained in Section III-D, Haptigami can generate a vibrotactile feedback by alternating its motors rotations at high speed. We powered the top motor at a range of frequencies between 10 and 300 Hz, which correspond to the maximum human perception frequency [59], and measured the force amplitude using the 6-axis load-cell.

Fig. 7d shows the measured peak-to-peak force difference for the various tested frequencies. Other than the small peak at around 220 Hz, the force characteristics seem constant across the frequency range, with a mean value of 451 mN and a standard deviation of 73 mN. While we tested only the top motor here, we believe that using both motors will increase the force amplitude.

TABLE II
TABLE SUMMARIZING THE MAXIMUM NORMAL, SHEAR AND VIBROTACTILE FORCE CAPACITY OF OUR DEVICE.

	Force (mN)		
	Pitch shear	Roll shear	Normal
Pitch motor	121	387	572
Roll motor	38	85	235
Two motors	159	407	693

Compression: 679 mN
One motor vibration amplitude peak: 664 mN

VI. CONCLUSION AND FUTURE WORK

Producing multiple degrees of mechanical stimulation from a wearable fingertip haptic platform is challenging. Generating a realistic user experience for any haptic interface demands embedding several mechanical functionalities at the centimeter scale which inevitably pushes the limit of physical and material structural mechanics. Here, we present Haptigami, a novel concept and design of a compact and wearable haptic device that renders cutaneous and vibrotactile feedback. Using only two low-profile piezomotors, it is able to generate compression, roll, pitch and vibrotactile feedback, which create a diverse range of haptic sensations including contact and pressure display, curvature display, shear forces, stiffness and vibration and texture. The use of piezomotors, along with the low-profile mechanisms, introduces a new approach in the manufacturing of low-profile, lightweight and compliant wearable devices. We derived and validated a model for the kinematics of Haptigami prototype. Based on the size of the finger, the kinematics model can be adapted to achieve closed-loop position control. In order to quantitatively assess mechanical performance, we developed a novel experimental protocol and platform to characterize the forces applied by Haptigami in its range of motion. The Haptigami provides forces ranging from 150 to 690 mN in different actuation modes, which are greater than the human skin perception threshold of around 41 mN as described by [60]. Using these values, we can model the force output of the Haptigami as a function of its kinematic orientation and inputs, in order to implement force or stiffness control. In addition to the novel design approach, we addressed another challenge in the existing literature, related to quantifying haptic feedback. Our presented method of force characterization is complete and comprehensive, providing a repeatable and consistent method of measuring the various modes of actuation in the entire range of motion of the Haptigami. This could be applied to other existing or upcoming mesoscale devices for characterizing their mechanical behaviour. By comparing different devices and by additionally conducting user studies, we would be able to link and quantify the relation between mechanical output of a meso-scale haptic device to the result of a psychophysical experiment.

Due to its size and compliance to the finger, Haptigami has multiple uses. In addition to virtual reality applications, it can provide haptic feedback for object manipulation or in general interaction with a physical environment. It could help to orientate hands in space for reaching an invisible target (e.g. in surgery [61] or assisting blind people). Finally, having both force and position feedback directly at the fingertip augments our ability to manipulate objects [62] in terms of precision and environmental perception by enhancing the perceived sensations.

Our future work will define an optimized design process for what design is optimal for a specific finger size in order to customize Haptigami to its user. Additionally, we will study different Haptigami elements such as piezomotors, mechanisms and materials; and design parameters such as

origami-structural stiffness, friction, electric signal frequency and power for improving haptic performance. Furthermore, using Inertial Measurement Units (IMUs), we will implement further closed-loop position control for the pitch and roll motions. Using the data from our characterization, we will develop models for Haptigami force output in order to implement force control. Lastly, we will test the device on several users to better understand the relation between applied the forces and haptic feedback.

REFERENCES

[1] J. Cannan and H. Hu, "Human-machine interaction (hmi): A survey," *University of Essex*, 2011.

[2] T. Rose, C. S. Nam, and K. B. Chen, "Immersion of virtual reality for rehabilitation-review," *Applied ergonomics*, vol. 69, pp. 153–161, 2018.

[3] N. Jafari, K. D. Adams, and M. Tavakoli, "Haptics to improve task performance in people with disabilities: A review of previous studies and a guide to future research with children with disabilities," *Journal of rehabilitation and assistive technologies engineering*, vol. 3, p. 2055668316668147, 2016.

[4] D. P. Losey, C. G. McDonald, E. Battaglia, and M. K. O'Malley, "A review of intent detection, arbitration, and communication aspects of shared control for physical human–robot interaction," *Applied Mechanics Reviews*, vol. 70, no. 1, p. 010804, 2018.

[5] N. C. Nilsson, S. Serafin, F. Steinicke, and R. Nordahl, "Natural walking in virtual reality: A review," *Computers in Entertainment (CIE)*, vol. 16, no. 2, p. 8, 2018.

[6] C. Pacchierotti, S. Sinclair, M. Solazzi, A. Frisoli, V. Hayward, and D. Prattichizzo, "Wearable haptic systems for the fingertip and the hand: taxonomy, review, and perspectives," *IEEE transactions on haptics*, vol. 10, no. 4, pp. 580–600, 2017.

[7] T. Hulin, M. Rothammer, I. Tannert, S. S. Giri, B. Pleintinger, H. Singh, B. Weber, and C. Ott, "Fingertac–a wearable tactile thimble for mobile haptic augmented reality applications," in *International Conference on Human-Computer Interaction*. Springer, 2020, pp. 286–298.

[8] H. A. Sonar, A. P. Gerratt, S. P. Lacour, and J. Paik, "Closed-loop haptic feedback control using a self-sensing soft pneumatic actuator skin," *Soft robotics*, vol. 7, no. 1, pp. 22–29, 2020.

[9] C. Pacchierotti, A. Tirmizi, and D. Prattichizzo, "Improving transparency in teleoperation by means of cutaneous tactile force feedback," *ACM Transactions on Applied Perception (TAP)*, vol. 11, no. 1, pp. 1–16, 2014.

[10] F. Chinello, M. Malvezzi, C. Pacchierotti, and D. Prattichizzo, "Design and development of a 3rrs wearable fingertip cutaneous device," in *2015 IEEE International Conference on Advanced Intelligent Mechatronics (AIM)*. IEEE, 2015, pp. 293–298.

[11] D. Leonardis, M. Solazzi, I. Bortone, and A. Frisoli, "A wearable fingertip haptic device with 3 dof asymmetric 3-rsr kinematics," in *2015 IEEE World Haptics Conference (WHC)*. IEEE, 2015, pp. 388–393.

[12] S. B. Schorr and A. M. Okamura, "Three-dimensional skin deformation as force substitution: Wearable device design and performance during haptic exploration of virtual environments," *IEEE transactions on haptics*, vol. 10, no. 3, pp. 418–430, 2017.

[13] F. Chinello, C. Pacchierotti, M. Malvezzi, and D. Prattichizzo, "A three revolute-revolute-spherical wearable fingertip cutaneous device for stiffness rendering," *IEEE Transactions on Haptics*, vol. 11, no. 1, pp. 39–50, 2018.

[14] Y. Mo, A. Song, and H. Qin, "Analysis and performance evaluation of a 3-dof wearable fingertip device for haptic applications," *IEEE Access*, vol. 7, pp. 170 430–170 441, 2019.

[15] F. Chinello, M. Malvezzi, D. Prattichizzo, and C. Pacchierotti, "A modular wearable finger interface for cutaneous and kinesthetic interaction: control and evaluation," *IEEE Transactions on Industrial Electronics*, vol. 67, no. 1, pp. 706–716, 2019.

[16] E. M. Young and K. J. Kuchenbecker, "Implementation of a 6-dof parallel continuum manipulator for delivering fingertip tactile cues," *IEEE transactions on haptics*, vol. 12, no. 3, pp. 295–306, 2019.

[17] M. Gabardi, M. Solazzi, D. Leonardis, and A. Frisoli, "A new wearable fingertip haptic interface for the rendering of virtual shapes and surface features," in *2016 IEEE Haptics Symposium (HAPTICS)*. IEEE, 2016, pp. 140–146.

[18] H. Culbertson, S. B. Schorr, and A. M. Okamura, "Haptics: The present and future of artificial touch sensation," *Annual Review of Control, Robotics, and Autonomous Systems*, vol. 1, pp. 385–409, 2018.

[19] D. Leonardis, M. Solazzi, I. Bortone, and A. Frisoli, "A 3-rsr haptic wearable device for rendering fingertip contact forces," *IEEE transactions on haptics*, vol. 10, no. 3, pp. 305–316, 2016.

[20] A. Firouzeh, Y. Sun, H. Lee, and J. Paik, "Sensor and actuator integrated low-profile robotic origami," in *2013 IEEE/RSJ International Conference on Intelligent Robots and Systems*. Ieee, 2013, pp. 4937–4944.

[21] A. Firouzeh and J. Paik, "Robogami: A fully integrated low-profile robotic origami," *Journal of Mechanisms and Robotics*, vol. 7, no. 2, p. 021009, 2015.

[22] J. Paik, "Soft robot design methodology for 'push-button'manufacturing," *Nature Reviews Materials*, vol. 3, no. 6, p. 81, 2018.

[23] R. Wood, S. Avadhanula, R. Sahai, E. Steltz, and R. Fearing, "Microrobot design using fiber reinforced composites," *Journal of Mechanical Design*, vol. 130, no. 5, p. 052304, 2008.

[24] Z. Zhakypov, K. Mori, K. Hosoda, and J. Paik, "Designing minimal and scalable insect-inspired multi-locomotion millirobots," *Nature*, vol. 571, no. 7765, pp. 381–386, 2019.

[25] Z. Zhakypov and J. Paik, "Design methodology for constructing multi-material origami robots and machines," *IEEE Transactions on Robotics*, vol. 34, no. 1, pp. 151–165, 2018.

[26] J.-L. Huang, Z. Zhakypov, H. Sonar, and J. Paik, "A reconfigurable interactive interface for controlling robotic origami in virtual environments," *The International Journal of Robotics Research*, vol. 37, no. 6, pp. 629–647, 2018.

[27] S. Mintchev, M. Salerno, A. Cherpillod, S. Scaduto, and J. Paik, "A portable three-degrees-of-freedom force feedback origami robot for human–robot interactions," *Nature Machine Intelligence*, vol. 1, no. 12, pp. 584–593, 2019.

[28] F. H. Giraud, Z. Zhakypov, and J. Paik, "Design of low-profile compliant transmission mechanisms," in *2019 IEEE/RSJ International Conference on Intelligent Robots and Systems (IROS)*. IEEE, 2019, pp. 2700–2707.

[29] "Pcbmotor website," https://pcbmotor.com/.

[30] H. Ellesgaard, E. Johansen, T. Olesen, H. Andersen, and M. H. Hansen, "Electro-mechanical wave device," May 25 2010, uS Patent 7,723,900.

[31] S. Scheggi, L. Meli, C. Pacchierotti, and D. Prattichizzo, "Touch the virtual reality: using the leap motion controller for hand tracking and wearable tactile devices for immersive haptic rendering," in *ACM SIGGRAPH 2015 Posters*, 2015, pp. 1–1.

[32] D. Tsetserukou, S. Hosokawa, and K. Terashima, "Linktouch: A wearable haptic device with five-bar linkage mechanism for presentation of two-dof force feedback at the fingerpad," in *2014 IEEE Haptics Symposium (HAPTICS)*. IEEE, 2014, pp. 307–312.

[33] M. Solazzi, A. Frisoli, and M. Bergamasco, "Design of a novel finger haptic interface for contact and orientation display," in *2010 IEEE Haptics Symposium*. IEEE, 2010, pp. 129–132.

[34] D. Prattichizzo, F. Chinello, C. Pacchierotti, and M. Malvezzi, "Towards wearability in fingertip haptics: a 3-dof wearable device for cutaneous force feedback," *IEEE Transactions on Haptics*, vol. 6, no. 4, pp. 506–516, 2013.

[35] I. Sarakoglou, N. G. Tsagarakis, and D. G. Caldwell, "A compact tactile display suitable for integration in vr and teleoperation," in *2012 IEEE International Conference on Robotics and Automation*. IEEE, 2012, pp. 1018–1024.

[36] S.-C. Kim, C.-H. Kim, G.-H. Yang, T.-H. Yang, B.-K. Han, S.-C. Kang, and D.-S. Kwon, "Small and lightweight tactile display (salt) and its application," in *World Haptics 2009-Third Joint EuroHaptics conference and Symposium on Haptic Interfaces for Virtual Environment and Teleoperator Systems*. IEEE, 2009, pp. 69–74.

[37] G. Frediani, D. Mazzei, D. E. De Rossi, and F. Carpi, "Wearable wireless tactile display for virtual interactions with soft bodies," *Frontiers in bioengineering and biotechnology*, vol. 2, p. 31, 2014.

[38] I. M. Koo, K. Jung, J. C. Koo, J.-D. Nam, Y. K. Lee, and H. R. Choi, "Development of soft-actuator-based wearable tactile display," *IEEE Transactions on Robotics*, vol. 24, no. 3, pp. 549–558, 2008.

[39] K. Minamizawa, S. Fukamachi, H. Kajimoto, N. Kawakami, and S. Tachi, "Gravity grabber: wearable haptic display to present virtual mass sensation," in *ACM SIGGRAPH 2007 emerging technologies*, 2007, pp. 8–es.

[40] M. Bianchi, E. Battaglia, M. Poggiani, S. Ciotti, and A. Bicchi, "A wearable fabric-based display for haptic multi-cue delivery," in *2016 IEEE haptics symposium (HAPTICS)*. IEEE, 2016, pp. 277–283.

[41] A. Frisoli, M. Solazzi, F. Salsedo, and M. Bergamasco, "A fingertip haptic display for improving curvature discrimination," *Presence: Teleoperators and Virtual Environments*, vol. 17, no. 6, pp. 550–561, 2008.
[42] B. T. Gleeson, S. K. Horschel, and W. R. Provancher, "Design of a fingertip-mounted tactile display with tangential skin displacement feedback," *IEEE Transactions on Haptics*, vol. 3, no. 4, pp. 297–301, 2010.
[43] A. Girard, M. Marchal, F. Gosselin, A. Chabrier, F. Louveau, and A. Lécuyer, "Haptip: Displaying haptic shear forces at the fingertips for multi-finger interaction in virtual environments," *Frontiers in ICT*, vol. 3, p. 6, 2016.
[44] M. Hosseini, Y. Pane, A. Sengül, J. De Schutter, and H. Bruyninckx, "A novel haptic glove (exoten-glove) based on twisted string actuation (tsa) system for virtual reality," in *International Conference on Human Haptic Sensing and Touch Enabled Computer Applications*. Springer, 2018, pp. 612–622.
[45] R. Fagiani, F. Massi, E. Chatelet, Y. Berthier, and A. Akay, "Tactile perception by friction induced vibrations," *Tribology International*, vol. 44, no. 10, pp. 1100–1110, 2011.
[46] S. Pabon, E. Sotgiu, R. Leonardi, C. Brancolini, O. Portillo-Rodriguez, A. Frisoli, and M. Bergamasco, "A data-glove with vibro-tactile stimulators for virtual social interaction and rehabilitation," in *10th Annual Intl Workshop on Presence*, 2007, pp. 345–348.
[47] F. Sanfilippo, L. I. Hatledal, and K. Pettersen, "A fully–immersive hapto–audio–visual framework for remote touch," in *Proc. IEEE International Conference on Innovations in Information Technology*, 2015.
[48] J. Foottit, D. Brown, S. Marks, and A. M. Connor, "Development of a wearable haptic game interface," *arXiv preprint arXiv:1604.08322*, 2016.
[49] Y. Chen, H. Feng, J. Ma, R. Peng, and Z. You, "Symmetric waterbomb origami," *Proceedings of the Royal Society A: Mathematical, Physical and Engineering Sciences*, vol. 472, no. 2190, p. 20150846, 2016.
[50] J. Bezanson, A. Edelman, S. Karpinski, and V. B. Shah, "Julia: A fresh approach to numerical computing," *SIAM review*, vol. 59, no. 1, pp. 65–98, 2017. [Online]. Available: https://doi.org/10.1137/141000671
[51] M. Salerno, K. Zhang, A. Menciassi, and J. S. Dai, "A novel 4-dof origami grasper with an sma-actuation system for minimally invasive surgery," *IEEE Transactions on Robotics*, vol. 32, no. 3, pp. 484–498, 2016.
[52] P. K. Mogensen, K. Carlsson, S. Villemot, S. Lyon, M. Gomez, C. Rackauckas, T. Holy, D. Widmann, T. Kelman, D. Karrasch, A. Levitt, A. N. Riseth, C. Lucibello, C. Kwon, D. Barton, J. TagBot, M. Baran, M. Lubin, S. Choudhury, S. Byrne, S. Christ, T. Arakaki, T. A. Bojesen, benneti, and M. R. G. Macedo, "Julianlsolvers/nlsolve.jl: v4.5.1," Dec. 2020. [Online]. Available: https://doi.org/10.5281/zenodo.4404703
[53] Maplesoft, a division of Waterloo Maple Inc., Waterloo, Ontario, "Maple," 2019. [Online]. Available: https://www.maplesoft.com/
[54] G. Bradski, "The OpenCV Library," *Dr. Dobb's Journal of Software Tools*, 2000.
[55] M. Kristan, A. Leonardis, J. Matas, M. Felsberg, R. Pflugfelder, L. Cehovin Zajc, T. Vojir, G. Hager, A. Lukezic, A. Eldesokey *et al.*, "The visual object tracking vot2017 challenge results," in *Proceedings of the IEEE international conference on computer vision workshops*, 2017, pp. 1949–1972.
[56] A. Abdouni, M. Djaghloul, C. Thieulin, R. Vargiolu, C. Pailler-Mattei, and H. Zahouani, "Biophysical properties of the human finger for touch comprehension: influences of ageing and gender," *Royal Society open science*, vol. 4, no. 8, p. 170321, 2017.
[57] B. M. Dzidek, M. J. Adams, J. W. Andrews, Z. Zhang, and S. A. Johnson, "Contact mechanics of the human finger pad under compressive loads," *Journal of The Royal Society Interface*, vol. 14, no. 127, p. 20160935, 2017.
[58] S. Joshi and J. Paik, "Multi-dof force characterization of soft actuators," *IEEE Robotics and Automation Letters*, vol. 4, no. 4, pp. 3679–3686, 2019.
[59] S. A. Wall and W. Harwin, "A high bandwidth interface for haptic human computer interaction," *Mechatronics*, vol. 11, no. 4, pp. 371–387, 2001.
[60] S. J. Lederman and R. L. Klatzky, "Sensing and displaying spatially distributed fingertip forces in haptic interfaces for teleoperator and virtual environment systems," *Presence: Teleoperators & Virtual Environments*, vol. 8, no. 1, pp. 86–103, 1999.
[61] A. Hein and M. Brell, "Contact-a vibrotactile display for computer aided surgery," in *Second Joint EuroHaptics Conference and Symposium on Haptic Interfaces for Virtual Environment and Teleoperator Systems (WHC'07)*. IEEE, 2007, pp. 531–536.
[62] I. M. Bullock and A. M. Dollar, "Classifying human manipulation behavior," in *2011 IEEE International Conference on Rehabilitation Robotics*. IEEE, 2011, pp. 1–6.

Frederic H. Giraud was born in Marseille, France in 1994. He received a M.S. degree in microelectronic and computer science from the Ecole des Mines de Saint-Etiennes in 2017. He is currently pursuing a Ph.D. degree in robotics at the Reconfigurable Robotics Laboratory (RRL) from Ecole Polytechnique Federale de Lausanne (EPFL) in Switzerland. His research interests include human-machine interface, haptic feedback, origami robotics, control strategies, manufacturing techniques, artificial intelligence and interactive VR simulations.

Sagar Joshi received the B.E. degree in mechanical engineering from Sardar Patel College of Engineering, Mumbai, India, in 2013, and the M.Tech. degree in Mechanical Engineering from the Indian Institute of Technology, Bombay, Mumbai, India, in 2016. Since 2016, he has been working in the Reconfigurable Robotics Laboratory at Ecole Polytechnique Federale de Lausanne (EPFL), where he is currently a Ph.D. student. His research interests include mechatronics, soft robots, wearable devices and biomechanics.

Jamie Paik received the Ph.D. degree in designing humanoid arm and a hand from Seoul National University, Seoul, South Korea. She is the Director and founder of Reconfigurable Robotics Laboratory (RRL), Ecole Polytechnique Federale de Lausanne (EPFL), Switzerland, and a core member of the Swiss NCCR Robotics Group. RRLs research leverages expertise in multimaterial fabrication and smart material actuation. During her Postdoctoral positions in Institut des Systems Intelligents et de Robotic, Universitat Pierre Marie Curie, Paris VI, France, she developed laparoscopic tools that are internationally patented and commercialized. At Harvard University's Microrobotics Laboratory, she started developing unconventional robots that push the physical limits of material and mechanisms. Her current research focuses on soft robotics and self-morphing Robogami (robotic origami) that transforms its planar shape to 2-D or 3-D by folding in predefined patterns and sequences, just like the paper art, origami.